# COMPREHENSIVE CHARACTERIZATION AND MODELING OF PLANAR ANISOTROPY IN STAINLESS STEEL SUS 304 FOR ACCURATE EARING PROFILE PREDICTION IN CIRCULAR CUP DRAWING PROCESSES

**Lai Dang Giang[1], Tran Duc Hoan[1*], Pham Quoc Tuan[2]**
*[1]Le Quy Don Technical University, [2]Blekinge Institute of Technology, Karlskrona, Sweden*

**ARTICLE INFO**

**Received:** 23/12/2023
**Revised:** 25/3//2024
**Published:** 25/3//2024

**KEYWORDS**

Earing profile
Planar anisotropy
SUS 304
Circular cup drawing
Non-associated flow rule

**ABSTRACT**

The deep drawing process of stainless steel SUS 304 plays a crucial role in the production of cover and package cases. The inherent anisotropy of the material significantly impacts the profile of the deformed part, posing challenges to manufacturing procedures. This research provides a comprehensive investigation of the planar anisotropy in stainless steel SUS 304. Constitutive modeling approaches, employing both associated and non-associated flow rules, using quadratic functions have been applied in the simulation process. These developed material models have been subsequently applied to simulate a cup drawing process, aiming to predict the earing profile of the deformed part. Experimental tests have been conducted to validate the accuracy of the numerical models. Comparative analysis revealed that, when calibrated with stress-based parameters, the prediction accuracy of the associated model surpasses that of alternative models. This study offers a reliable predictive tool for earing profile outcomes in circular cup drawing processes for stainless steel SUS 304.

# ĐẶC TÍNH TOÀN DIỆN VÀ MÔ HÌNH DỊ HƯỚNG PHẲNG CỦA THÉP KHÔNG GỈ SUS 304 ĐỂ DỰ ĐOÁN BIÊN DẠNG TAI CHÍNH XÁC TRONG QUÁ TRÌNH DẬP VUỐT CỐC TRÒN

**Lại Đăng Giang[1], Trần Đức Hoàn[1*], Phạm Quốc Tuấn[2]**
*[1]Trường Đại học Kỹ thuật Lê Quý Đôn, [2]Viện Công nghệ Blekinge, Karlskrona, Thụy Điển*

**THÔNG TIN BÀI BÁO**

**Ngày nhận bài:** 23/12/2023
**Ngày hoàn thiện:** 25/3//2024
**Ngày đăng:** 25/3//2024

**TỪ KHÓA**

Biên dạng tai
Dị hướng phẳng
SUS 304
Dập vuốt cốc tròn
Quy tắc chảy không liên tục

**TÓM TẮT**

Quá trình dập vuốt sâu thép không gỉ SUS 304 đóng vai trò quan trọng trong việc sản xuất các chi tiết dạng vỏ, hộp đựng. Tính dị hướng của vật liệu này tác động đáng kể đến hình dạng của chi tiết bị biến dạng, đặt ra thách thức trong quá trình sản xuất. Nghiên cứu này cung cấp một cái nhìn tổng quan về tính dị hướng phẳng trong thép không gỉ SUS 304. Các phương pháp mô hình hóa cấu thành dựa trên cả quy tắc dòng chảy liên tục và không liên tục, sử dụng các hàm bậc hai đã được áp dụng trong quá trình mô phỏng. Những mô hình vật liệu đã phát triển này sau đó được áp dụng để mô phỏng quá trình dập vuốt cốc tròn, nhằm mục đích dự đoán biên dạng tai của chi tiết bị biến dạng. Các thử nghiệm thực nghiệm được tiến hành để xác nhận tính chính xác của các mô hình số. Phân tích so sánh cho thấy rằng, khi được hiệu chỉnh bằng các tham số dựa trên ứng suất, độ chính xác dự đoán của mô hình liên kết sẽ vượt trội so với các mô hình khác. Nghiên cứu này cung cấp một công cụ dự đoán đáng tin cậy cho kết quả biên dạng tai trong quá trình dập vuốt cốc tròn đối với thép không gỉ SUS 304.

**DOI: https://doi.org/10.34238/tnu-jst.9469**

* Corresponding author. *Email: tranduchoan@lqdtu.edu.vn*

## 1. Introduction

Thin stainless steel sheets are widely used in covering and packaging industries [1]–[3] due to their extensive corrosion resistance and high formability. In these applications, the circular cup drawing is a common process for making parts. Designing products obtained from a cup drawing process requires accounting for several forming related phenomena such as wrinkling, earing, and failure [4], [5]. For this purpose, numerical simulation using the finite element (FE) method is an effective method to virtually analyze and save the cost. To ensure the capability of predicting the phenomena, a proper constitutive model is mandated in these simulations.

A constitutive model involves three essentials: a flow rule, a yield function, and a hardening law [6]–[8]. Common practice has been formulated following an associated flow rule in which the plastic strain increment is normal to the yield surface. Different functions have been proposed in literature to capture the anisotropic yield surface of sheet metals. For example, Hill [9] proposed the most common quadratic function; and, Hosford [10], [11] or Barlat et al. [12] proposed non-quadratic functions. The hardening law describes the rate of expansion of the yield surface due to the plastic deformation. Even though this modeling approach is widely used in practice, the identicality of yield and potential surfaces requires the use of a complex function to capture all experimental data.

Non-associated flow rule is an alternative in which the yield surface is separated to the potential surface. Within a same set of experimental data, the number of parameters involved to the yield function in this approach is less than that of the associative approach [13]–[15]. However, the use of these two approaches may lead to different simulated results due to the difference in their extrapolation to other stress states.

This study examines the application of these two modeling approaches in predicting the earing profile observed in the cup drawing of a stainless steel SUS304 sheet. Uniaxial tensile tests are conducted for specimens prepared in three different orientations to characterize the anisotropy of the tested material. Different material models based on both associated and non-associated flow rules are developed with the use of quadratic yield functions. The developed models are employed to simulate the cup drawing of the tested material. The predicted earing profile and thickness distribution are compared to the experimental measurements. Based on the comparisons, the usefulness of these models is discussed.

## 2. Methodology

### *2.1. Experiment*

#### *2.1.1. Uniaxial tensile tests*

A stainless steel SUS304 sheet with a thickness of 0.8 mm was investigated in this study. The tested material has been widely used in different engineering fields, such as civil, building, ship, automotive and aerospace. Uniaxial tensile tests were conducted following the standard ISO 6892-1:2019 for specimens prepared in differential orientations such as Rolling direction (RD), diagonal direction (DD) and transversal direction (TD). During experimental tests, a constant crosshead speed of 3 mm/min was applied to pull the testing specimen until failure. The loads acting on the specimen were recorded by a loadcell; and the displacement of an initial gauge length of 10 mm was recorded by an extensometer. Based on the measured force-displacement data, the engineering and true stress-strain data were derived straightforwardly.

Additional tensile tests were conducted up to 10% of engineering strain to measure the Lankford values or R-value. The value is determined from a uniaxial tensile test as follow:

$$R = \frac{\varepsilon_w}{\varepsilon_t} \quad (1)$$

where $\varepsilon_w$ and $\varepsilon_t$ denote the strain measured in width and thickness directions of the deformed uniaxial tensile specimen. The Lankford value is well-known to be influenced to material's responses during deep drawing processes.

*2.1.2. Circular cup drawing test*

Manufacturing cylinder parts require one or more deep drawing processes of a circular blank sheet. In this study, a circular cup drawing test was conducted for SUS304 sheet with an initial diameter of 100 mm. Figure 1 shows tool's geometries used in the test. The heights of wall region were measured at several points to estimate the earing profile of the deformed specimen.

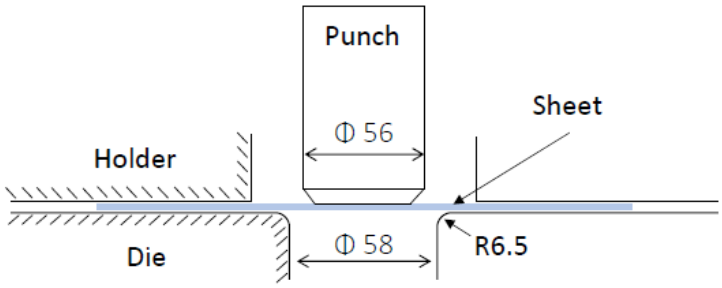


**Figure 1**. *Tool geometries for circular cup drawing test (dimensions in mm)*

### *2.2. Constitutive model and Finite element model*

In this study, a hardening law recently proposed by Pham and Kim [6] was adopted to describe the hardening behavior of the tested material. The formulation of this model is expressed as following:

$$H(\bar{\varepsilon}) = c_1 + c_2(1 - \exp(-c_3\bar{\varepsilon}))(0.002 + \bar{\varepsilon})^{c_4} \quad (2)$$

where $c_1 \sim c_4$ are material's parameters that should be calibrated. Herein, a common curve fitting method [16] was applied to identify these parameters.

A yield function is needed to govern material's behavior in multi-axial stress states. The most common isotropic yield function is the one proposed by Mises, of which formulation is expressed as:

Mises
$$\bar{\sigma}(\boldsymbol{\sigma}) = \sqrt{\sigma_{11}^2 + \sigma_{22}^2 - \sigma_{11}\sigma_{22} + 3\sigma_{12}^2} \quad (3)$$

In order to take material's anisotropy into account, Hill's quadratic function [17] is adopted for this purpose due to its simplicity. The formulation of Hill's quadratic function is expressed as follows:

Hill48
$$\bar{\sigma}(\boldsymbol{\sigma}) = \sqrt{G\sigma_{11}^2 + F\sigma_{22}^2 - H\sigma_{11}\sigma_{22} + 2N\sigma_{12}^2} \quad (4)$$

where $G, F, H, N$ are material's parameters, which can be identified from experimental data.

There are different methods used to determine parameters of a Hill's quadratic function. In the one hand, these parameters are determined from the Lankford values, from which the function is labeled by "Hill-R", as follows:

Hill-R
$$G = \frac{1}{1 + R_0}$$
$$F = \frac{R_0}{(1 + R_0)R_{90}}$$
$$H = \frac{R_0}{1 + R_0} \quad (5)$$
$$N = \frac{(1 + 2R_{45})(R_0 + R_{90})}{2R_{90}(1 + R_0)}$$

where $R_0, R_{45}, R_{90}$ are the measured Lankford values of the RD, DD, and TD specimens, respectively. In another hand, these parameters are determined from stress ratios, from which the function is labeled by "Hill-S", as follows:

$$\text{Hill-S} \quad \begin{aligned} G &= \frac{1}{2}\left(\frac{1}{\sigma_0^2} - \frac{1}{\sigma_{90}^2} + \frac{1}{\sigma_b^2}\right) \\ F &= \frac{1}{2}\left(-\frac{1}{\sigma_0^2} + \frac{1}{\sigma_{90}^2} + \frac{1}{\sigma_b^2}\right) \\ H &= \frac{1}{2}\left(\frac{1}{\sigma_0^2} + \frac{1}{\sigma_{90}^2} - \frac{1}{\sigma_b^2}\right) \\ N &= \frac{1}{2}\left(\frac{4}{\sigma_{45}^2} - \frac{1}{\sigma_b^2}\right) \end{aligned} \tag{6}$$

where $\sigma_0, \sigma_{45}, \sigma_{90}$ are the stress ratios obtained from uniaxial tensile tests in RD, DD, and TD, respectively; $\sigma_b$ denotes the ratio between the equi-biaxial stress and $\sigma_0$. In this study, $\sigma_b = 1$ is assumed due to the lack of experimental test in the equi-biaxial stress state. The value of $\sigma_b$ is selected by referring measured results of SUS304 sheet materials published in literature [11], [12], [18]. A finite element model was developed in Abaqus/Explicit package [19] to simulate the cup drawing process of SuS304 sheet. Finite element model of cup drawing simulation was presented in the Figure 2.

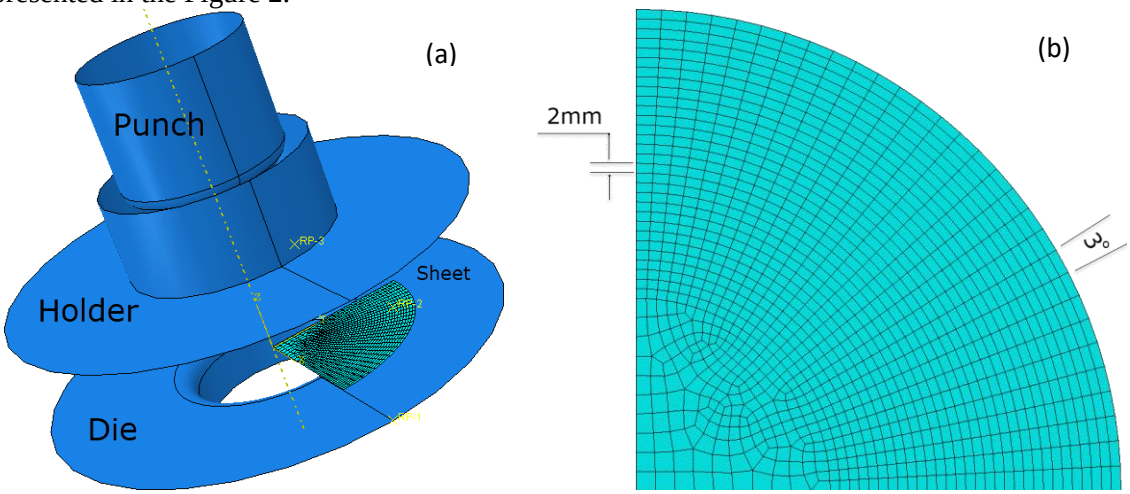


**Figure 2.** *Finite element model of cup drawing simulation (a) Assembly and (b) Mesh on the sheet*

Four-node shell elements with reduced integration (S4R) were employed to model the sheet. Analytical rigid body element was used to model the tools. Figure 5 shows mesh generation on the sheet used in simulations. In detail, an increment of 2° in the circumferential direction and 1 mm in the radial direction was generated. The surface-to-surface algorithm available in Abaqus/explicit library was adopted to describe interactions during simulation. Following the recommendation of previous study [24], the Mohr-Coulomb friction model with a constant coefficient of 0.1 was applied to describe all contact pairs between tools and sheet. Constitutive equations described in the previous section were implemented in a user's subroutine VUMAT to describe material's behavior during the cup drawing process.

## 3. Results and Disccusion

Figure 3 shows stress-strain curves obtained from uniaxial tensile tests. The difference in these stress-strain curves indicates material anisotropy, which is critical for the tested material as shown in Figure 3(a). Furthermore, the ultimate tensile strength (UTS) in the engineering curves points out the initiation of diffuse neck. Beyond the UTS, material is deformed largely before

failure, which verifies the importance of post-necking hardening behavior on material's responses. The obtained stress-strain curves exhibit similarities to those reported in tensile tests of the stainless steel SUS304 sheet with a thickness of 1.2 mm and a crosshead speed of 5 mm/min [20]. The observation is attributed to the minor influence of crosshead speed and specimen size on the stress-strain curves under similar experimental conditions in cold plastic deformation.

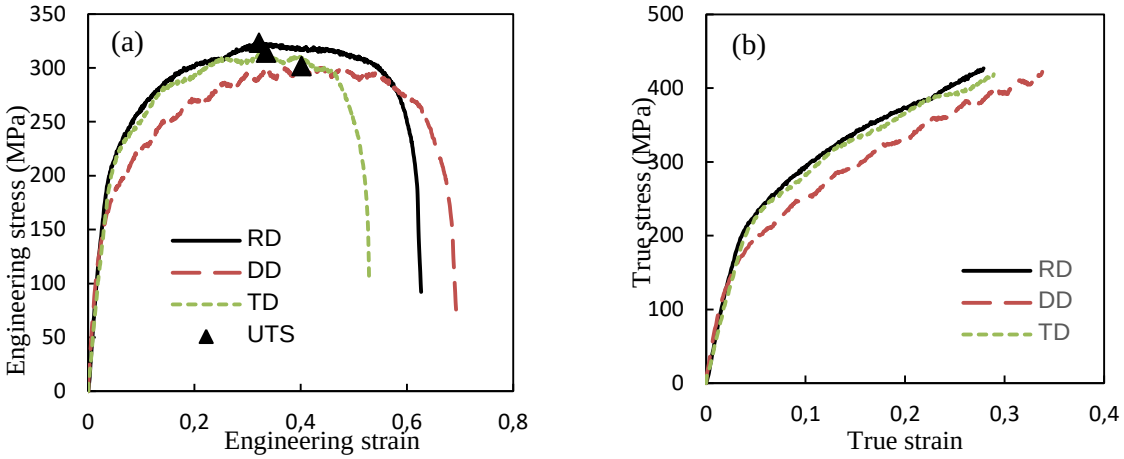


**Figure 3**. *Stress-strain curves obtained from uniaxial tensile tests: (a) Engineering stress-strain curves and (b) True stress-strain curves*

Figure 4 shows a comparison between the calibrated hardening law and the experimental data obtained from the uniaxial tensile test conducted for the RD specimen. It is seen that the identified hardening laws provides excellent match to the experimental data.

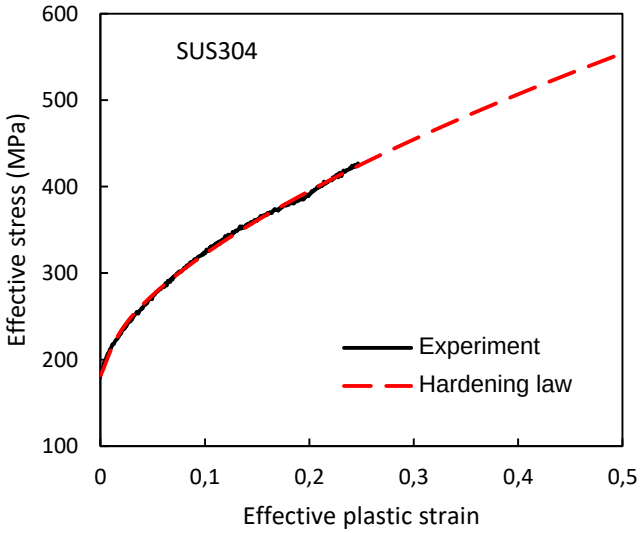


**Figure 4**. *Identified hardening law for SUS304 sheet material*

Table 1 reports material properties obtained from these uniaxial tensile tests. Significant differences in Lankfords values and stress ratios determined in different orientations shown in Table 1 raise challenges in predicting the earring profile observed in the cup drawing test of the investigated material.

The identified parameters of hardening law and yield functions are reported in Table 2.

**Table 1.** *Material properties obtained from uniaxial tensile tests*

| | Rolling direction | Diagonal direction | Transversal direction |
|---|---|---|---|
| Yield stress (MPa) | 182.32 | 151.15 | 171.10 |
| Stress ratio | 1 | 0.9145 | 0.9818 |
| Ultimate tensile strength (MPa) | 323.02 | 301.21 | 313.80 |
| Lankford value | 1.29 | 0.86 | 0.67 |
| Elongation (%) | 62.6 | 69.3 | 52.8 |

**Table 2.** *Calibrated parameters of the constitutive equations*

| Yield function | G | H | F | N |
|---|---|---|---|---|
| Hill-R | 0.4363 | 0.5637 | 0.8377 | 1.7353 |
| Hill-S | 0.4813 | 0.5187 | 0.5187 | 1.8915 |
| Hardening law | $c_1$ (MPa) | $c_2$ (MPa) | $c_3$ | $c_4$ |
| Lankford value | 182.0 | 567.93 | 149.1 | 0.613 |

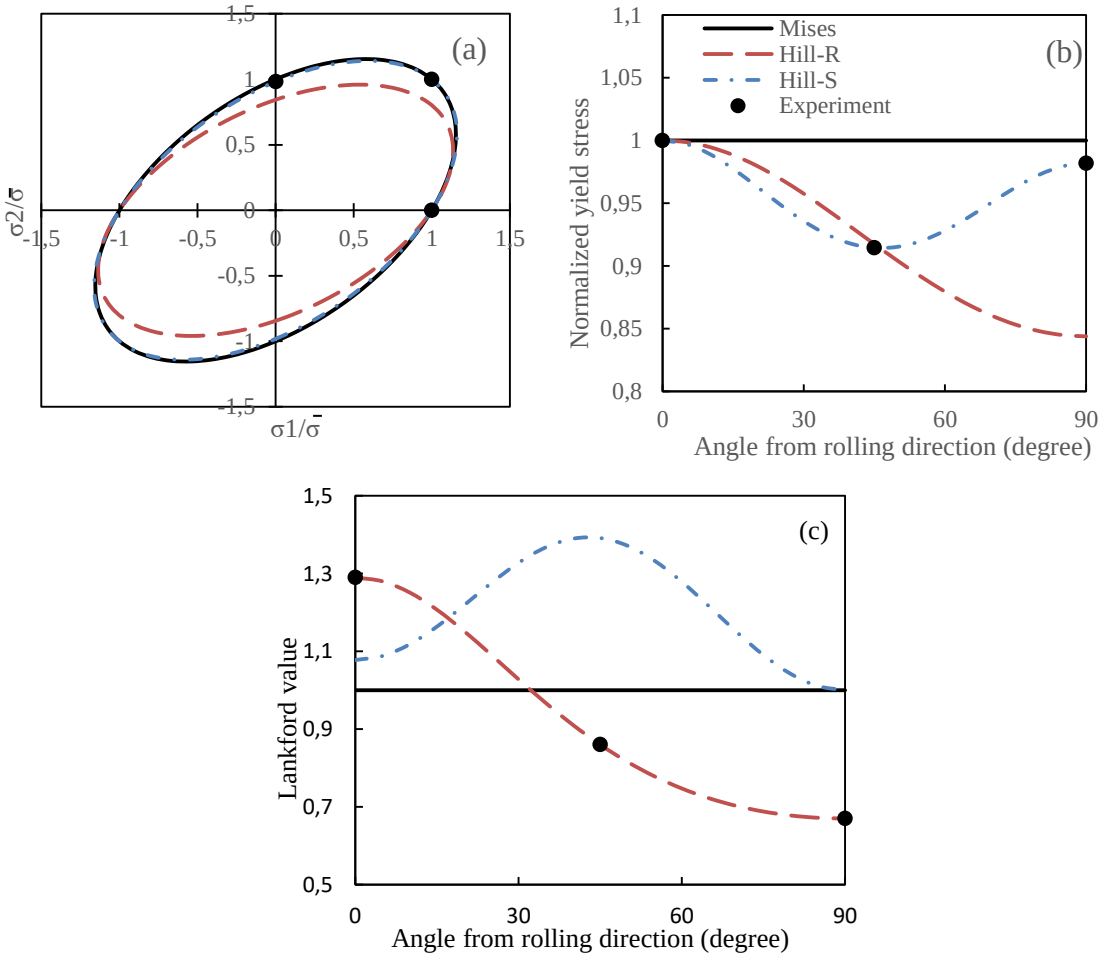


**Figure 4.** *Comparison between different yield functions and experimental data (a) Yield locus (b) Normalized yield stress and (c) Lankford value*

As seen in Table 2, different calculation methods provide different values of parameters. Therefore, Figure 4 compares their applications with the measured data. Furthermore, relevant

calculation results of Mises yield function are also plotted in these figures for comparisons. It is seen that the Hill-S function provides a similar yield locus to those of Mises function. Naturally, Hill-S and Hill-R functions yield good evaluations for normalized yield stress and Lankford value, respectively because they used the considering experimental data in the formulation. However, the application of Hill-S function for Lankford value as well as the application of Hill-R function for normalized yield stress show significant deviations. The difference is due to the limitation of Hill's quadratic function and was reported in detail in references [17], [21].

Under plastic deformation, the yield condition is expressed as:

$$f(\boldsymbol{\sigma}, \bar{\varepsilon}) = \bar{\sigma}(\boldsymbol{\sigma}) - H(\bar{\varepsilon}) \leq 0 \quad (7)$$

where $f(\boldsymbol{\sigma}, \bar{\varepsilon})$ is the yield surface. During the calculation, a flow rule provides the increment of plastic strain components as the follows:

$$d\varepsilon_{ij}^{p} = d\lambda \frac{\partial g(\boldsymbol{\sigma}, \bar{\varepsilon})}{\partial \sigma_{ij}} \quad (8)$$

where $\lambda$ is the plastic multiplier, $g(\boldsymbol{\sigma}, \bar{\varepsilon})$ is the potential surface.

Commonly, an associated flow rule is employed in finite element analyses, where the potential surface is identical to the yield surface. Recently, a non-associated flow rule has been proposed, where the yield and potential surface is separated numerically [22]. The usefulness of the proposal was discussed in reference [23]. This study adopted both associated and non-associated flow rules to model three cup drawing process of SUS304 sheet. In the former approach, Hill-S and Hill-R functions can be used for both yield and potential surfaces, leading to two different simulations. The latter approach, Hill-S function is adopted for modeling the yield surface and Hill-R function is adopted for the potential surface modeling.

Figure 5 shows a comparison of thickness distribution on the deformed specimens obtained from different material models. It is seen that the predicted thickness distribution is strongly sensitive to the employed material model. In detail, the use of Mises model yields the same thickness prediction in all orientations. On the cup's edge, Hill-R and Hill-NAFR models predict a strong variation in the thickness of elements located in the RD and TD; while, a less sensitivity in the thickness distribution is observed in the case of Hill-S model. The comparison clarifies the effect of material modeling on the numerical predictions.

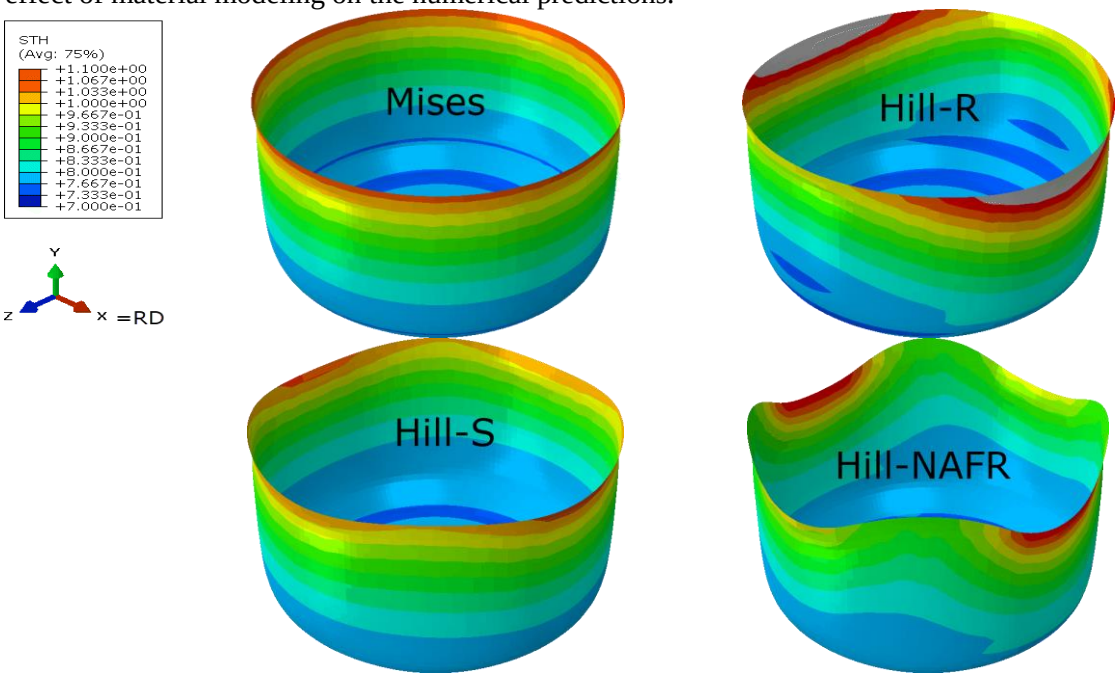


**Figure 5**. *Predictions of thickness distribution on the deformed specimen based on different material models*

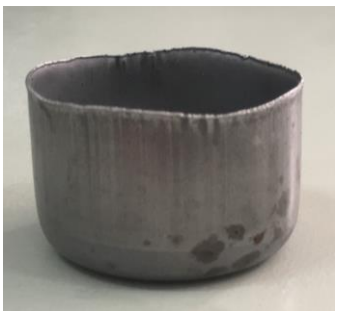

**Figure 6**. *Circular cup drawing test: A deformed specimen*

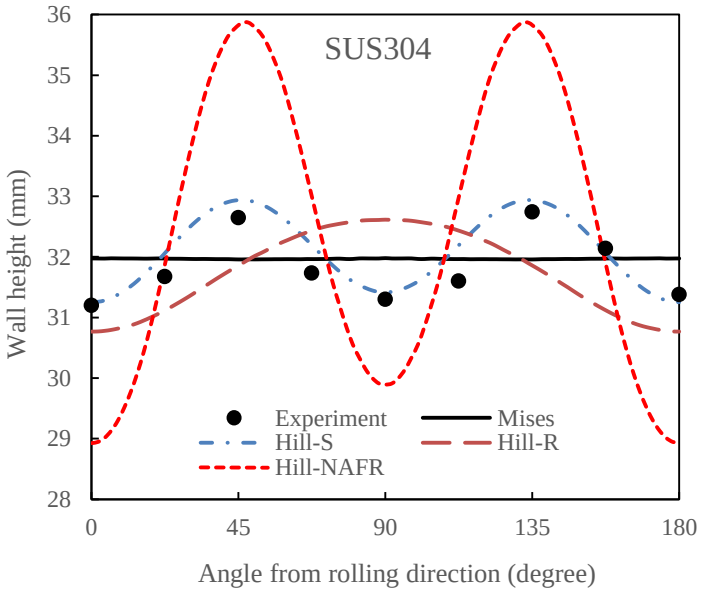


**Figure 7**. *Comparison of the measured and predicted wall height of the deformed SUS304 cup*

Figure 6 shows a deformed specimen obtained from the Circular cup drawing test. The deformed specimen exhibits four ears with low height in the diagonal direction. The mouth part of the specimen tends to wrinkle, a phenomenon explained by the fact that compressive circumferential stress attains its maximum value at the outer profile of the circular blank sheet.

Figure 7 compares the predictions of earing profile of these material models with the experimental measurement. As seen in this figure, the measurement results indicate four ears occurred in the diagonal direction. The use of Mises yield function provides a typical prediction for the earing profile. Hill-R predicts the highest wall height at 90° from the RD, which is deviated from the measured data. Predictions of Hill-S function for both the maximum wall height and earing profile are in an agreement well with the experimental data. The maximum wall height error of Hill-S prediction compared to the experiment is 0.63%. Comparing the results of Hill-S model, use of NAFR approach (Hilll-NAFR) does not increase the accuracy of earing prediction. The later gives a correct prediction of ear orientation but its prediction for the wall height variation is too strong. Noted that the observed overestimation of earing behavior is also reported in several studies for different materials with NAFR approach [7], [24]. The reason for the mismatch is due to the calibration procedure of NAFR model that introduced too strict constraints on the uniaxial tension forming mode. However, the forming mode dominated the deformation of circular cup drawing process is the one combined between the compressive circumferential and tensile radial stresses [25]. Care should be taken in modeling a material with non-associated flow rule approach for circular cup drawing simulation.

## 4. Conclusion

This study examined the ability of associative and non-associative modeling approaches in simulating the circular cup drawing test of SUS304 sheets. These material models were developed with quadratic yield and potential functions coupling with an isotropic hardening law proposed by Pham and Kim [10]. The performance of these models was accessed by comparing their predictions of earing profile with experimental measured data. It is seen that the stress-based calibrated model with the associated flow rule gives the best prediction for earing behavior of the tested material. In particular, using the Hill-S model gives the most consistent results with the

experimental data on the number, height, and direction appearance of the ear. The maximum wall height error in comparison to the experimental findings is notably minimal, standing at 0.63%. The non-associated flow rule provides correct prediction for the orientation of the maximum wall height but overestimates the wall height variation. A material model developed under non-associated flow rule approach should be used with care to achieve accurate prediction for the cup drawing process.

## REFERENCES

[1] G. K. Deshwal and N. R. Panjagari, "Review on metal packaging: materials, forms, food applications, safety and recyclability," *J. Food Sci. Technol.*, vol. 57, no. 7, pp. 2377–2392, 2020, doi: 10.1007/s13197-019-04172-z.

[2] T. C. Chen, J. C. Lin, and R. M. Lee, "Analysis of deep drawing process for stainless steel micro-channel array," *Materials (Basel).*, vol. 10, no. 4, pp. 12–14, 2017, doi: 10.3390/ma10040423.

[3] T. C. Chen, C. M. Hsu, and C. C. Wang, "The deep drawing of a flanged square hole in thin stainless steel sheet," *Metals (Basel).*, vol. 11, no. 9, 2021, doi: 10.3390/met11091436.

[4] T. Altan and A. E. Tekkaya, *Sheet Metal Forming: Processes and Applications*. ASM International, 2012.

[5] K. Chen, A. J. Carter, and Y. P. Korkolis, "Flange Wrinkling in Deep-Drawing: Experiments, Simulations and a Reduced-Order Model †," *J. Manuf. Mater. Process.*, vol. 6, no. 4, 2022, doi: 10.3390/jmmp6040076.

[6] Q. T. Pham and Y. S. Kim, "Identification of the plastic deformation characteristics of AL5052-O sheet based on the non-associated flow rule," *Met. Mater. Int.*, vol. 23, no. 2, pp. 254–263, 2017, doi: 10.1007/s12540-017-6378-5.

[7] H. Hippke, N. Manopulo, J. W. Yoon, and P. Hora, "On the efficiency and accuracy of stress integration algorithms for constitutive models based on non-associated flow rule," *Int. J. Mater. Form.*, vol. 11, no. 2, pp. 239–246, 2018, doi: 10.1007/s12289-017-1347-6.

[8] G. Chen, Z. Ke, C. Ren, and J. Li, "Constitutive modeling for Ti-6Al-4V alloy machining based on the SHPB tests and simulation," *Chinese J. Mech. Eng. (English Ed.*, vol. 29, no. 5, pp. 962–970, 2016, doi: 10.3901/CJME.2016.0406.046.

[9] R. Hill, "A theory of the yielding and plastic flow of anisotropic metals," *Proc. R. Soc. London, Ser. A*, vol. 193, no. 1033, pp. 281–297, 1948.

[10] Q. T. Pham and Y. S. Kim, "Evaluation on Flexibility of Phenomenological Hardening Law for Automotive Sheet Metals," *Metals (Basel).*, vol. 12, no. 4, pp. 1–19, 2022, doi: 10.3390/met12040578.

[11] W. F. Hosford, "A generalized isotropic yield criterion," *J. Appl. Mech. Trans. ASME*, vol. 39, no. 2, pp. 607–609, 1972, doi: 10.1115/1.3422732.

[12] F. Barlat *et al.*, "Plane stress yield function for aluminum alloy sheets - Part 1: Theory," *Int. J. Plast.*, vol. 19, no. 9, pp. 1297–1319, 2003, doi: 10.1016/S0749-6419(02)00019-0.

[13] E. Lee, T. B. Stoughton, and J. W. Yoon, "A yield criterion through coupling of quadratic and non-quadratic functions for anisotropic hardening with non-associated flow rule," *Int. J. Plast.*, 2017, doi: 10.1016/j.ijplas.2017.08.007.

[14] N. Park, T. B. Stoughton, and J. Whan, "A criterion for general description of anisotropic hardening considering strength differential effect with non-associated flow rule," *Int. J. Plast.*, vol. 121, no. April, pp. 76–100, 2019, doi: 10.1016/j.ijplas.2019.04.015.

[15] M. Safaei, J. Whan, and W. De Waele, "Study on the definition of equivalent plastic strain under non-associated flow rule for finite element formulation," *Int. J. Plast.*, vol. 58, pp. 219–238, 2014, doi: 10.1016/j.ijplas.2013.09.010.

[16] ABAQUS 6.14, *ANALYSIS USER'S GUIDE, Volume III*. Providence, Rhode Island: Dassault Systèmes Simulia Corp., 2014.

[17] D. Banabic *et al.*, *Sheet metal forming processes: Constitutive modelling and numerical simulation*. Springer, 2010.

[18] B. M. L. Zheng, C. Cheng, and M. Wan, "Experimental characterization and theoretical modeling of size-dependent distortional hardening behavior of ultrathin metal sheets under multi-axial loading," *Eur. J. Mech. - A/Solids*, vol. 92, 2022, doi: 10.1016/j.euromechsol.2021.104461.

[19] T. B. Stoughton and J. W. Yoon, "Anisotropic hardening and non-associated flow in proportional

loading of sheet metals," *Int. J. Plast.*, vol. 25, no. 9, pp. 1777–1817, 2009, doi: 10.1016/j.ijplas.2009.02.003.

[20] D. G. Lai, D. H. Tran, Q. D. Le, and V. C. Nguyen, "The effect of technology parameters on the size of the 'ear' when deep drawing for the first time of anisotropic cylindrical simulation," *J. Sci. Tech. - Le Quy Don Tech. Univ.*, vol. 18, no. 02, pp. 5–15, 2023, doi: 10.56651/lqdtu.jst. v18.n02.683.

[21] L. Luo, D. Wei, G. Zu, and Z. Jiang, "Influence of blank holder-die gap on micro-deep drawing of SUS304 cups," *Int. J. Mech. Sci.*, vol. 191, 2021, Art. no. 106065, doi: 10.1016/j.ijmecsci. 2020.106065.

[22] S. N. Yuan *et al.*, "Study on size effects in micro deep drawing of stainless steel foil," *J. Phys. Conf. Ser.*, vol. 2020, no. 1, 2021, doi: 10.1088/1742-6596/2020/1/012040.

[23]F. Barlat, J. W. Yoon, and O. Cazacu, "On linear transformations of stress tensors for the description of plastic anisotropy," *Int. J. Plast.*, vol. 23, no. 5, pp. 876–896, 2007, doi: 10.1016/j.ijplas.2006.10.001.

[24] B. Wu, K. Ito, N. Mori, T. Oya, T. Taylor, and J. Yanagimoto, "Constitutive Equations Based on Non-associated Flow Rule for the Analysis of Forming of Anisotropic Sheet Metals," *Int. J. Precis. Eng. Manuf. - Green Technol.*, vol. 7, no. 2, pp. 465–480, 2020, doi: 10.1007/s40684-019-00032-5.

[25] K. Chung, D. Kim, and T. Park, "Analytical derivation of earing in circular cup drawing based on simple tension properties," *Eur. J. Mech. A/Solids*, vol. 30, no. 3, pp. 275–280, 2011, doi: 10.1016/j.euromechsol.2011.01.006.